THE JOURNAL OF PHYSICAL CHEMISTRY C
A JOURNAL OF THE AMERICAN CHEMICAL SOCIETY

pubs.acs.org/JPCC

Article

Bimetallic Cu/Rh Catalyst for Preferential Oxidation of CO in H_2: a DFT Study

Published as part of The Journal of Physical Chemistry virtual special issue "Energy and Catalysis in China".

Chuwei Zhu, Xiang-Kui Gu,* and Wei-Xue Li*

Cite This: *J. Phys. Chem. C* 2021, 125, 19697−19705

Read Online

ABSTRACT: Preferential oxidation of CO in excess H_2 (PROX) has been extensively explored for selective removal of CO with minimum H_2 consumption to prevent CO poisoning of the Pt-based anode in a proton-exchange-membrane fuel cell (PEMFC). Unmodified platinum group metal catalysts are widely used for this reaction, yet they still show unsatisfying activity for CO oxidation at low temperatures, because their stronger adsorption of CO would poison the active site. Cu-based catalysts are alternatives, but they suffer from structural instability. Therefore, designing a more efficient catalyst for PROX is highly required. In this work, a bimetallic Cu/Rh catalyst is designed that facilitates significantly weakening the CO poisoning effect due to its comparable adsorption strengths of O_2 and CO. As compared to the dissociative mechanism, CO oxidation via the OCOO-mediated associative mechanism on this catalyst is found to be more favorable, and the barriers of the steps in the catalytic cycle are modest, suggesting a high low-temperature activity for CO oxidation. Moreover, it is found that a Cu/Rh catalyst exhibits lower selectivity for H_2 oxidation than that for CO oxidation. Additionally, the systematic studies of the surface segregation of Cu/Rh induced by the adsorption of species in PROX show that a Cu/Rh catalyst exhibits a good structural stability under the typical PROX conditions. These results demonstrate that the designed bimetallic Cu/Rh catalyst is promising for the PROX reaction at low temperatures.

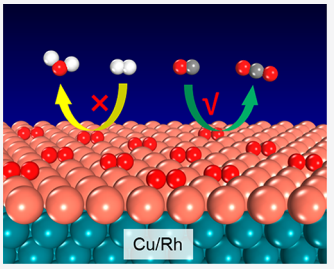

1. INTRODUCTION

Proton-exchange-membrane fuel cells (PEMFCs) that efficiently convert chemical energy to electric energy have attracted considerable attention as an alternative power source for vehicles and other applications.[1] These electrochemical devices utilize H_2 as a fuel for the anode reaction, while the traditionally used Pt electrocatalysts can be seriously poisoned by a CO byproduct derived from the current mainly used H_2 production processes, such as reforming of hydrocarbons.[2,3] To purify H_2, preferential oxidation of CO in excess H_2 (PROX) while minimizing H_2 consumption is a promising technology,[4,5] while the development of more active and selective catalysts exhibiting efficient performance at the operating temperatures of PEMFCs (~80 °C) remains a challenge. As a typical kind of monometallic catalyst for the PROX reaction,[6,7] supported platinum group metal (PGM) nanoparticles (e.g., Ru, Rh, Pt, Ir) have been widely studied. However, CO oxidation on these unmodified PGM catalysts requires a relatively high temperature (>120 °C),[8−19] because their much stronger CO adsorption would lead to a limited free active site for O_2 adsorption and dissociation. Enhanced catalytic activity of PGMs at low temperature by promoters has been intensively studied, such as reducible metal oxides,[20−29] alkali cations,[13,30−34] and the second metallic component.[35−45]

Cu-based catalysts are promising alternatives for the PROX reaction due to their abundance, accessibility, and low cost. Moreover, different from PGMs, the unique oxophilicity of Cu is effective for its active site free from CO poisoning at low temperatures. However, Cu-based catalysts suffer from their instability owing to the well-known sintering of Cu nanoparticles at their Hüttig temperature,[46−48] leading to a significant decrease in the content of their surface active sites and, consequently, a low CO conversion at low temperatures.[49−57] On the other hand, the metallic Cu is facially to be oxidized to Cu^+ or Cu^{2+} cations under PROX reaction conditions, which also impacts its activity and ambiguates the active phase.[56,58−63] Therefore, maintaining the structural stability and chemical state of Cu-based catalysts is crucial for their long-term applications. Fabricating bimetallic core−shell structure via depositing an overlayer of active Cu component on a second metal substrate with a stronger Cu-metal bond formation is a potential way to prevent the sintering of Cu. Meanwhile, in this structure, the ligand effect from the different orbital hybridization and the strain effect from the lattice difference also provide an opportunity in manipulating the reactivity of Cu. Additionally, the uniform surface structure

Received: May 27, 2021
Revised: August 9, 2021
Published: September 1, 2021

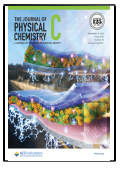

https://doi.org/10.1021/acs.jpcc.1c04645
J. Phys. Chem. C 2021, 125, 19697−19705

of Cu overlayer catalyst takes advantage of exposing larger amounts of identical active sites as compared to the supported catalysts with interface being the active site.

In this work, a bimetallic Cu/Rh(111) overlayer structure by supporting a copper monolayer on Rh(111) is constructed, and its catalytic performance for the PROX reaction is investigated and compared with Rh(111) and Cu(111). The energetics associated with the elementary steps for CO oxidation occurring via dissociative and associative mechanisms are calculated using density functional theory to study the activity of CO oxidation. The energetic comparison between CO oxidation and H_2 oxidation is used to determine the catalytic selectivity. The energetics of the surface segregation with and without adsorbate inducing are systematically calculated to determine the structural stability of the promising Cu/Rh.

2. COMPUTATIONAL METHODS

Periodic density functional theory (DFT) calculations were performed using Vienna Ab Initio Simulation Package (VASP). The Perdew–Burke–Ernzerhof (PBE) functional[64] within the generalized gradient approximation (GGA) regime was used to describe the electron exchange-correlation interaction. The core–valence interactions were modeled with the projector augmented wave (PAW) method.[65,66] The Kohn–Sham equations were solved in a plane wave basis set with a kinetic energy cutoff of 400 eV. The convergence criteria for the electronic self-consistent iteration and force were set to be 10^{-4} eV and 0.02 eV/Å, respectively. Transition states were located using the climbing image nudged elastic band (CI-NEB)[67,68] and dimer[69] methods. The convergence criterion was 0.05 eV/Å and the obtained saddle points were verified to have only one vibrational mode with a negative curvature in the direction of bond forming or breaking process.

To model the Rh@Cu catalyst with a core–shell structure, a five-layer Cu/Rh(111) slab was constructed including a monolayer (ML) Cu supported on a four-layer Rh(111) with a (2 × 2) unit cell. The five-layer slabs of Rh(111) and Cu(111) were also constructed as comparable systems. For the stability assessment and surface segregation evaluation induced by adsorbates at different coverages, a series of slab models of (111) surfaces with different unit cells were utilized. Models including one adsorbate in a (3 × 3), one in (2 × 2), one in (2 × 1), and two in (2 × 1) unit cells were used for the coverages of 1/9, 1/4, 1/2, and 1 ML, respectively. During the optimization, the bottom two layers were fixed in their bulk position whereas the other layers and adsorbates were allowed to relax. A 20 Å vacuum was introduced with correction of dipole moment between the artificially repeated slabs. The Brillouin zone was sampled by a (7 × 7 × 1) k-point mesh. The adsorption energies were calculated as

$$E_{ads}(\text{molec}) = E_{\text{molec/slab}} - E_{\text{slab}} - E_{\text{molec(g)}}$$

where $E_{\text{molec/slab}}$, E_{slab}, and $E_{\text{molec(g)}}$ are the total energies of adsorbed system, clean slab and adsorbate in the gas phase, respectively. The activation barrier (E_a) and reaction energy (E_r) were calculated with respect to the separately adsorbed species.

3. RESULTS AND DISCUSSION

3.1. Adsorption Properties. The calculated adsorption energies of reactants, intermediates, and products involved in PROX on Rh(111), Cu(111), and bimetallic Cu/Rh(111) are listed in Table 1, and the optimized corresponding geometries are shown in Figure S1. It is generally found that Rh exhibits the strongest adsorption, while Cu is the weakest. This is because the intrinsic activity of Rh is higher than Cu. As mentioned above, the competitive adsorption of CO and O_2 is crucial for the efficient PROX at low temperatures. On Rh(111), Table 1 clearly shows that the adsorption strength of CO (−1.95 eV) is stronger by 0.43 eV than that of O_2 (−1.52 eV), indicating that the active site would be mainly covered by CO, leading to a limited active site for O_2 adsorption and dissociation and a lower activity for CO oxidation at low temperatures. On Cu(111), it is found that the adsorption of CO (−0.83 eV) is just slightly stronger than that of O_2 (−0.70 eV), suggesting that the CO poisoning on the Cu catalyst can be significantly weakened as compared to that on the Rh catalyst. Nevertheless, the adsorption strengths of CO and O_2 reactants on Cu(111) are remarkably weaker than that on Rh(111), implying that their adsorption and the subsequent activation would be relatively challenging, affecting the entire PROX performance. In addition, the Cu catalyst can also suffer from its poor structural stability under the operating conditions.[47,52,70,71] These suggest that pure Cu is not a potential efficient catalyst for PROX.

Table 1. Calculated Most Stable Adsorption Energies (in eV) of Species Involved in the PROX Reaction on Rh(111), Cu(111), and Cu/Rh(111) Surfaces[a]

species	Rh(111)	Cu(111)	Cu/Rh(111)
CO	−1.95	−0.83	−1.09
O_2	−1.52	−0.70	−1.04
O	−2.13	−1.68	−1.91
CO_2	−0.02	−0.01	−0.02
H	−0.55	−0.21	−0.34
OH	−3.10	−3.07	−3.47
H_2O	−0.31	−0.15	−0.22

[a]The adsorption energies of atomic O and H are with respect to 1/2O_2 and 1/2H_2 in the gas phase, respectively.

As compared to Cu(111), Cu/Rh(111) exhibits a stronger adsorption strength, providing a relatively sufficient driving force for CO and O_2 species adsorption and activation, leading to a potentially improved activity for PROX at low temperatures. More importantly, Cu/Rh(111) shows the comparable energetic nature for CO and O_2 competitive adsorption (−1.09 and −1.04 eV), facilitating to prevent CO poisoning the active site. These results indicate that Rh@Cu core–shell structured catalyst is promising for PROX. The stronger adsorption nature of Cu/Rh(111) than Cu stems from the lattice strain and ligand effects. The calculated in-plane Cu–Cu distance is 2.566 Å on Cu(111), while it is expanded by 5.38% on Cu/Rh(111) (2.704 Å), leading to a tensile strain effect. The ligand effect involves the heterometallic bonding interaction between the surface Cu and the underneath Rh atoms, which results in an orbital hybridization and charge redistribution on the interface of Cu and Rh (Figure S2). Both the strain effect and the ligand effect contribute to the modification of the electronic structure of the surface Cu, as evidenced by the calculated d-band center (−2.27 eV) of surface Cu on Cu(111) exhibiting an upshift toward the Fermi level to −2.00 eV for surface Cu on Cu/Rh(111). This d-band center

https://doi.org/10.1021/acs.jpcc.1c04645
J. Phys. Chem. C 2021, 125, 19697−19705

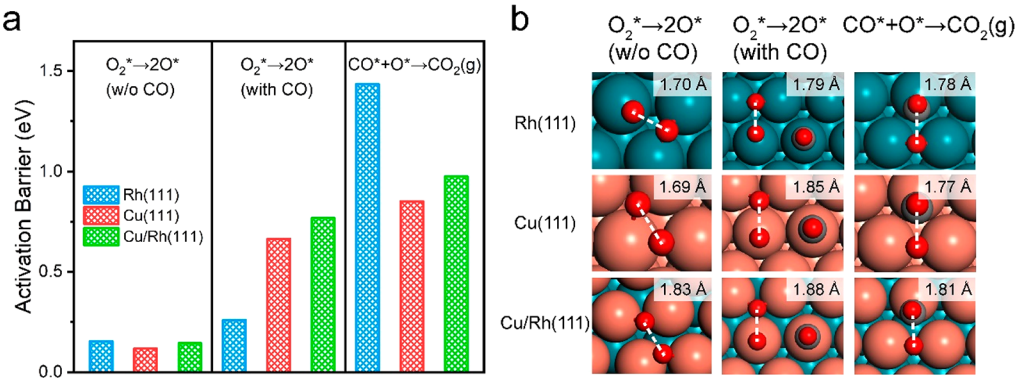

Figure 1. (a) Activation barriers for O_2 dissociation (without and with CO coadsorption) and CO_2 formation on Rh(111), Cu(111), and Cu/Rh(111) surfaces. (b) Optimized structures of transition states. The cyan, orange, gray, and red spheres represent Rh, Cu, C, and O atoms, respectively.

upshift results in a stronger adsorption for species on Cu/Rh(111) than that on Cu(111).

3.2. Activity of CO oxidation. *3.2.1. Dissociative Mechanism for CO Oxidation.* The dissociative mechanism for CO oxidation involves the direct dissociation of molecular O_2 to form the atomic O, followed by the CO reaction with atomic O to produce CO_2. The reaction energies and activation barriers associated with these two steps on Rh(111), Cu(111), and Cu/Rh(111) surfaces are shown in Figure 1 and Table S1. It is found that O_2 dissociation exhibits very low activation barriers (0.15, 0.12, and 0.14 eV on Rh(111), Cu(111) and Cu/Rh(111), respectively) on these clean surfaces (Figure 1a, left panel), due to the much exothermicity of this reaction on these systems (Table S1). The activation barriers for CO reaction with atomic O formed to produce CO_2 are much higher than that for O_2 dissociation (Figure 1a, right panel). On Cu(111) and Cu/Rh(111), the calculated respective activation barriers of 0.85 and 0.97 eV are modest, while the barrier of 1.44 eV on Rh(111) is much higher than that on Cu-based metal surfaces, owing to the stronger adsorption energies for CO and atomic O on Rh surface.

As compared to O_2, the CO reactant exhibits stronger or at least comparable adsorption strength on these surfaces, implying that the coadsorption of CO and O_2 is inevitable and the coexistence of CO on the surface would affect the dissociation of O_2. To study this effect, the activation barriers for O_2 dissociation with coadsorption of 1/4 ML CO on these surfaces are calculated for example (middle panel of Figure 1a and Table S1). As expected, the CO coadsorption can increase the dissociation barrier. In the case of Rh(111), it is found that the O_2 dissociation barrier is higher by 0.11 eV on the CO coadsorbed surface than that on the clean surface, and the similar transition states are observed in both cases, where one oxygen atom is at the top site and the other one is at the bridge site (Figure 1b). The slight increase in the O_2 dissociation barrier on the CO coadsorbed Rh(111) surface mainly stems from the fact that O_2 is more activated in the transition state with a longer O−O bond distance (1.79 Å) than that on a clean Rh surface. On Cu(111) and Cu/Rh(111), the CO coadsorption can significantly increase the O_2 dissociation barriers by 0.54 and 0.63 eV, respectively, due to the CO coadsorption can change the transition state structures. In the transition states for O_2 dissociation on the clean Cu(111) and Cu/Rh(111), the two oxygen atoms are both located at two adjacent bridge sites with an O−O distance of 1.69 and 1.83 Å, respectively (Figure 1b). On CO coadsorbed surfaces with a CO molecule at a top site, the transition state involves one atomic O at a fcc hollow site and the other one at a top site. It is expected that the O_2 dissociation barrier would further increase with an increase in the coverage of coadsorbed CO.[72,73] While it is found that the maximum CO coverage on Cu-based catalysts, such as on Cu/Rh(111), is 1/4 ML under the typical PROX conditions (the same coverage used here), as discussed below. This suggests that the reaction of CO with atomic O is still the rate-determining step for CO oxidation via dissociative mechanism on CO coadsorbed Cu-based metal surfaces. Moreover, the relative lower barriers for CO reaction with atomic O on Cu(111) and Cu/Rh(111) than that on Rh(111) suggest that the Cu-based catalysts are promising for PROX at lower temperatures.

3.2.2. Associative Mechanism for CO Oxidation. The CO coadsorption on the surface will decrease the amount of free active site for O_2 dissociation, limiting the O_2 direct dissociation to two atomic oxygen, which requires more free active surface sites. Thus, an alternative associative mechanism for CO oxidation is considered on the promising Cu(111) and Cu/Rh(111). In this mechanism, the molecularly adsorbed O_2 directly binds to CO to form OCOO species, followed by the scission of the O−O bond to produce an oxygen atom and a CO_2 molecule.[74−76] This will decrease the requirement of the number of free sites for O_2 dissociation, and the oxygen atom formed can react with a second CO molecule. On Cu(111), the O−O bond distance in OCOO transition state is elongated to 1.66 Å, which is longer by 14.5% than that in an adsorbed O_2 molecule (Figure 2a). The length of the C−O bond formed is 1.47 Å and the O−O−C angle is 104.86°. On Cu/Rh(111), the O−O bond is elongated to 1.69 Å in the OCOO transition state, and the formed C−O bond length is 1.47 Å with the O−O−C angle to be 107.22°. The more activated O−O bond on Cu/Rh(111) results in a slightly higher barrier of 0.58 eV for OCOO formation, as compared to that of 0.51 eV on Cu(111). The further O−O bond elongation of OCOO to produce CO_2 is a barrierless process. We note that these barriers are lower than that for the direct dissociation of O_2 on CO coadsorbed corresponding surfaces and that for the CO reaction with O on Cu and Cu/Rh surfaces (Figure 2b).

3.2.3. Catalytic Cycle for CO Oxidation. To better understand the energetics associated with CO oxidation via dissociative and associative mechanisms on the promising

https://doi.org/10.1021/acs.jpcc.1c04645
J. Phys. Chem. C 2021, 125, 19697−19705

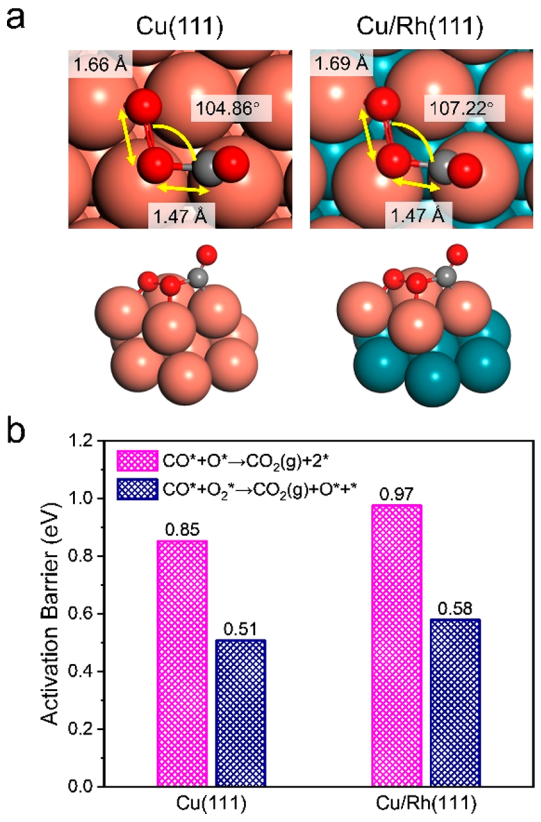

Figure 2. (a) Top and side views of optimized structures of OCOO transition state for CO oxidation via associative mechanism on Cu(111) and Cu/Rh(111). The cyan, orange, gray, and red spheres represent Rh, Cu, C, and O atoms, respectively. (b) Comparison of activation barriers for CO reaction with atomic O in dissociative mechanism and OCOO formation in associative mechanism.

Cu(111) and Cu/Rh(111) surfaces, the energy profiles and catalytic cycles are shown in Figures 3 and S3. For CO oxidation via a dissociative mechanism, it is found that both O_2 dissociation and CO reaction with atomic O are exothermic processes, while the barrier of CO reaction with atomic O is higher than that of O_2 dissociation on CO coadsorbed surface. For the associative mechanism, the second CO_2 formation is the same as that in the dissociative mechanism. However, the first CO_2 formation via the OCOO transition state exhibits much lower barriers than the CO reaction with atomic O in the dissociative mechanism, demonstrating that the first CO_2 formation via associative mechanism is much more favorable. On the other hand, using the coadsorbed CO and O_2 as the reference state, it is found that the effective barrier (the highest energy height in the energy profile) that comes from the CO direct binding to O_2 for the associative mechanism (0.58 eV) is lower than that for the dissociative mechanism (0.77 eV). Thus, CO oxidation through the associative mechanism in the entire catalytic cycle is more facile. As a comparison of the barriers for CO oxidation via the facile associative mechanism on Cu(111) and Cu/Rh(111), it is found that the barriers on Cu(111) is slightly lower than that on Cu/Rh(111), suggesting that the activity of CO oxidation on pure metallic Cu catalyst is slightly higher than bimetallic Cu/Rh catalyst. While maintaining the metallic state of Cu is very challenging under PROX conditions, the Cu/Rh catalyst might be more appropriate.

3.3. Selectivity of PROX. The highly selective oxidation of CO rather than H_2 in the reaction atmosphere of PROX is crucial to minimize H_2 consumption during CO removal. Thus, the energetics associated with H_2 oxidation to H_2O are calculated (Table S1 and Figure S4) and compared with those associated with CO oxidation. It is found that H_2 dissociation on Rh(111) is a barrierless process, while the calculated barriers for H_2 dissociation on Cu(111) and Cu/Rh(111) are 0.61 and 0.39 eV, respectively. For an atomic H reaction with an atomic O to form OH, the calculated barriers on Rh(111), Cu(111), and Cu/Rh(111) are 1.29, 1.14, and 1.17 eV, respectively. This is because the atomic O and H exhibit the strongest adsorption on Rh(111), while the weakest on Cu(111). In the case of OH reaction with H to produce

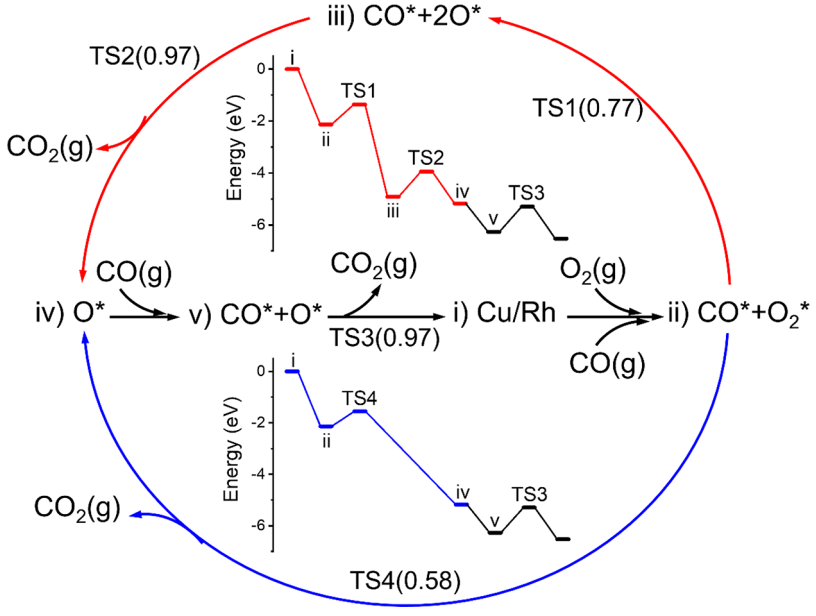

Figure 3. Potential energy profiles and catalytic cycles for CO oxidation via dissociative (red lines) and associative mechanisms (blue lines) on Cu/Rh(111).

https://doi.org/10.1021/acs.jpcc.1c04645
J. Phys. Chem. C 2021, 125, 19697−19705

H_2O, it is found that the barrier of 1.37 eV on Cu/Rh(111) is higher than that of 1.05 and 0.92 eV on Cu(111) and Rh(111), respectively. These results demonstrate that the reaction between OH and H is the rate-determining step for H_2 oxidation to H_2O on Cu/Rh(111), while the atomic H reaction with atomic O is the rate-determining step on Cu(111) and Rh(111) (Figure 4a). As a comparison of the barriers of the rate-determining steps for CO and H_2 oxidation (Figure 4b), it is clear that the activity of CO oxidation is higher than H_2 oxidation on Cu/Rh(111), owing to the barrier of 0.97 eV for the CO reaction with O being lower than that of 1.37 eV for the OH reaction with H by 0.40 eV and suggests a high selectivity toward CO oxidation. In the case of Cu(111), the barrier of CO reaction with O (0.85 eV) is lower than that of atomic O reaction with H (1.14 eV) by 0.29 eV, also suggesting a preferential oxidation of CO instead of H_2. However, Rh(111) exhibits a higher activity for H_2 oxidation, since the rate-determining reaction of O and H shows a lower barrier (1.29 eV) than CO reaction with O (1.44 eV). These results indicate that the Cu/Rh catalyst is the most promising for PROX, with the highest selectivity toward CO oxidation, while Rh catalyst shows the highest selectivity for H_2 oxidation.

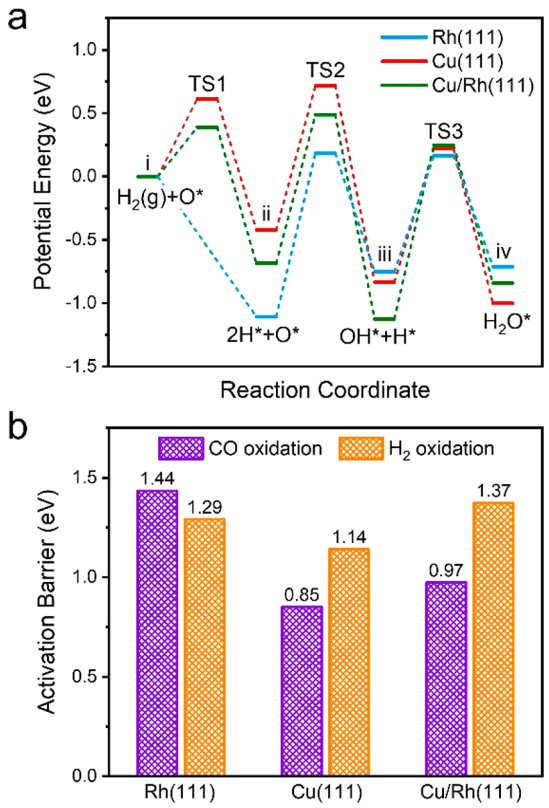

Figure 4. (a) Potential energy diagrams of H_2 oxidation on Rh(111), Cu(111), and Cu/Rh(111) surfaces. (b) Comparison of activation barriers of rate-determining steps in CO oxidation and H_2 oxidation on these surfaces.

3.4. Stability of Bimetallic Cu/Rh(111). The structural stability of the most promising Cu/Rh(111) is another crucial factor for its practical application in PROX. To explore the structural stability, the surface segregation of bimetallic Cu/Rh(111) is studied. Initially, the energetic change induced by Rh component outward diffusion from subsurface or bulk region to surface layer via exchanging with surface Cu is calculated. Figure S5 depicts a monotonic energy increase when the surface Cu atoms exchange with the subsurface Rh atoms, demonstrating a thermodynamically unfavorable process of Rh enrichment on the surface layer. The position exchanges of all nine Cu−Rh pairs in a (3 × 3)-supercell can form a sandwich-like Rh/Cu/Rh(111) structure with a Cu subsurface layer, resulting in an average energy increase of 0.28 eV per Cu−Rh pair exchange. This result is consistent with the segregation energy of −0.38 eV for a Cu atom segregation from the bulk to the surface in the RhCu system.[77] Figure S6 illustrates a more energy requirement for inward diffusion of surface Cu to the deeper bulk region. For instance, a surface Cu atom inward diffusion to the fifth atomistic layer is endothermic by 0.86 eV, which agrees with −0.99 eV for Cu diffusion from the core to the outermost corner site in a 55-atom Cu@Rh binary alloy nanoparticle.[78] These results evidently demonstrate that segregation of subsurface Rh atoms onto the outermost Cu layer is thermodynamically prohibitive.

On the other hand, the adsorbate-induced surface segregation is also studied, and the PROX intermediates of CO, O_2, O, OH, and H are considered as the adsorbates. The segregation energy (ΔE_s) is defined as the energy difference between adsorbates binding on Rh/Cu/Rh(111) and Cu/Rh(111) systems per (1 × 1) supercell:

$$-\Delta E_s = \frac{1}{N}(E_{\text{ads@Cu/Rh(111)}} - E_{\text{ads@Rh/Cu/Rh(111)}})$$

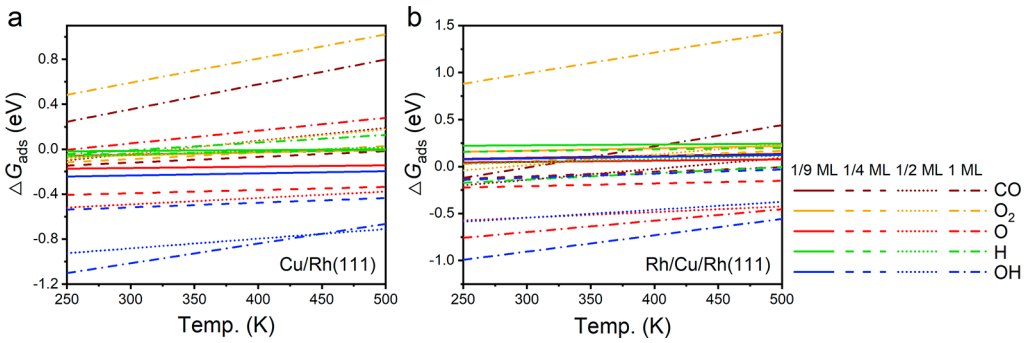

Figure 5. Surface-phase diagrams for PROX intermediate adsorption on Cu/Rh(111) and segregated Rh/Cu/Rh(111). The partial pressures of CO, O_2, and H_2 are assumed to be 10, 5, and 985 mbar, respectively. The adsorption free energies (ΔG_{ads}) of the O atom, H atom, and OH are relative to $1/2O_2$ and $1/2H_2$ in the gas phase.

https://doi.org/10.1021/acs.jpcc.1c04645
J. Phys. Chem. C 2021, 125, 19697−19705

$E_{ads@Rh/Cu/Rh(111)}$ and $E_{ads@Cu/Rh(111)}$ represent the total energies of adsorbed Rh/Cu/Rh(111) and Cu/Rh(111) systems. N equals 9, 4, 2, and 2 for the coverage of 1/9, 1/4, 1/2, and 1 ML, respectively. The positive segregation energy demonstrates an impossibility of adsorbate-induced segregation, while the negative value implies the existence of a thermodynamic driving force for the surface segregation due to the different affinity of adsorbates with Cu and Rh. First, the surface-phase diagrams are constructed for these intermediate adsorptions on Cu/Rh(111) and segregated Rh/Cu/Rh(111) with various coverages at temperature ranging from 250 to 500 K (Figures 5 and S7). Figure 5 shows that the OH-covered Cu/Rh(111) is the most thermodynamically stable; however, the formation of OH is kinetically challenging, owing to the high barrier of the O reaction with H, as discussed above. Considering the modest barrier for O_2 dissociation, and the second most stable nature of atomic O on the surface-phase diagram, the Cu/Rh(111) might be covered by 1/2 ML O. A similar stability trend of these intermediates on the segregated Rh/Cu/Rh(111) is also observed (Figure 5b), while their free energies are generally higher than those on Cu/Rh(111) at relatively lower coverage (less than 1/2 ML), implying that the adsorbate-induced surface segregation process is challenging. This is supported by the calculated positive segregation energies induced by the specific intermediate adsorption at 1/9 and 1/4 ML (Figure 6). The negative segregation energies are only obtained for CO

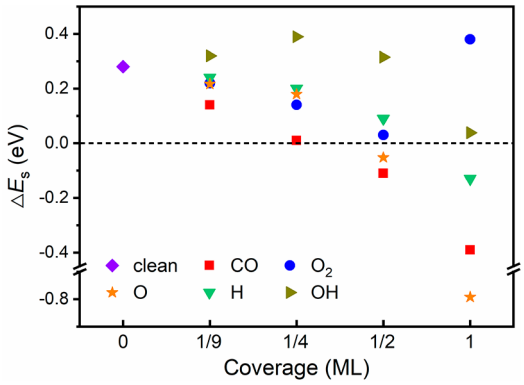

Figure 6. Adsorbate-induced segregation energy (ΔE_s) per (1 × 1) supercell at different coverages on the Cu/Rh(111) surface.

and O adsorption at 1/2 ML, as well as CO, O, and H adsorption at 1 ML. While Figure 5a shows that the maximum coverages for CO, O, and H are 1/4, 1/2, and 1/2 ML, respectively, suggesting that CO and H cannot induce a surface segregation. We note that the segregation energy induced by atomic O at its maximum coverage (1/2 ML) is only −0.05 eV. Considering the existence of kinetic barrier that has to be overcome for atom inward and outward diffusion during segregation, atomic O-induced surface segregation might hardly happen under realistic conditions.

In addition, Cu-based catalysts generally suffer from particle aggregation and dispersion decrease through Ostwald ripening or particle migration coalescence. It has been reported that Cu would lose one-third of its initial activity after 1000 h of operation, and sintering is the main reason.[70,71] For Cu/Rh(111), the binding energy between surface Cu and subsurface Rh is calculated to be −1.14 eV per Cu−Rh pair, which is stronger than that of −0.80 eV for each Cu−Cu pair in Cu(111). The stronger interaction between Cu and Rh can decrease the mobility of surface Cu, limiting the Cu sintering and oxidation. To further confirm this, Cu_2O overlayer formation and reduction on Cu/Rh(111) and Cu(111) are studied. Using two coadsorbed oxygen atoms on a (2 × 2) surface as the initial state (Figure S8), the Cu_2O overlayer can be formed through one adsorbed oxygen atom insertion into the subsurface region with half of surface Cu atoms uplifted. This process is exothermic by 0.61 and 0.20 eV on Cu(111) and Cu/Rh(111), respectively, indicating a more facile surface oxide formation on Cu and a relatively antioxidation capability of Cu/Rh(111). On the other hand, Cu_2O overlayer can be reduced by H_2 and CO under PROX condition. For instance, the Cu_2O partial reduction by H_2 to Cu_4O_1 is exothermic by 0.20 and 1.60 eV for Cu_2O/Cu(111) and Cu_2O/Rh(111), respectively, suggesting that the reduction of Cu_2O/Rh is much more favorable. It is worthy to note that the subsurface O atom in Cu_2O/Rh would move to the surface after the partial reduction, which can be removed via CO oxidation. While this O atom in Cu_2O/Cu still prefers to be located in the subsurface region. These results imply that the Cu/Rh(111) structure can be dynamically maintained during PROX.

The above results demonstrate that the Cu overlayer supported on a second metal is an effective strategy for designing an efficient PROX catalyst. To screen more promising candidates, the studies are extended to other Cu/TM (TM = Ni, Zn, Ru, Pd, Ir, Pt, Ag, Au) systems using the simple but key characters to estimate their stability and activity, such as the segregation energies of the subsurface TM atom exchange with the surface Cu atom, and the adsorption energies of CO and O_2. Among these it is found that Cu/Ni, Cu/Ru, and Cu/Ir exhibit positive segregation energies, suggesting that these catalysts are potentially stable, while the other catalysts considered are not stable due to their negative segregation energies (Table 2). Moreover, CO

Table 2. Calculated Segregation Energies (ΔE_s) of the Subsurface TM Atom Exchange with the Surface Cu Atom, as Well as the Adsorption Energies of CO (E_{ads}(CO)) and O_2 (E_{ads}(O_2)) on the Cu/TM Surface

Cu/TM	ΔE_s (eV) per (1 × 1) supercell	E_{ads}(CO) (eV)	E_{ads}(O_2) (eV)	lattice strain (%)
Cu/Ni(111)	0.22	−0.73	−0.66	−3.15
Cu/Zn(0001)	−0.41	−0.65	−0.88	3.55
Cu/Ru(0001)	0.88	−1.01	−1.31	5.81
Cu/Pd(111)	−0.22	−1.06	−1.34	8.46
Cu/Ir(111)	0.33	−1.06	−1.38	6.73
Cu/Pt(111)	−0.33	−1.10	−1.45	9.33
Cu/Ag(111)	−0.25	−1.04	−1.89	14.09
Cu/Au(111)	−0.49	−1.17	−1.91	14.50

adsorption on Cu/Ni is stronger than O_2 adsorption, indicating that the dissociation of O_2 would be hindered by the poison of CO. Therefore, except for Cu/Rh, Cu/Ru and Cu/Ir might also be promising candidates as active and stable PROX catalysts.

4. CONCLUSIONS

Density functional theory calculations are employed to study CO oxidation in excess H_2 on Rh(111), Cu(111), and Cu/Rh(111) surfaces. It is found that the stronger CO adsorption than O_2 on Rh(111) can lead to a CO poisoning for CO

https://doi.org/10.1021/acs.jpcc.1c04645
J. Phys. Chem. C 2021, 125, 19697−19705

oxidation on a Rh catalyst by hampering O_2 dissociation, while this poisoning effect can be significantly weakened on Cu and Cu/Rh catalysts due to their comparable adsorption strengths for CO and O_2. CO oxidation on Cu and Cu/Rh prefers the associative mechanism via an OCOO species as the transition state toward CO_2 formation, followed by the left atomic O reaction with a second CO. CO reaction with O is identified to be the rate-determining step for CO oxidation on these surfaces, and Rh exhibits the highest barrier, while Cu and Cu/Rh exhibit comparable modest barriers. For H_2 oxidation, it is found that the rate-determining step is a H reaction with O on Rh and Cu, whereas it is an OH reaction with H on Cu/Rh. More importantly, the activation barrier of the rate-determining step for H_2 oxidation on Cu/Rh is obviously higher than that for CO oxidation. However, an opposite trend is observed on Rh. These suggest that Cu/Rh exhibits a higher selectivity for CO oxidation, facilitating to minimize H_2 consumption during PROX. Furthermore, Cu/Rh shows a good structural stability under typical PROX conditions. These results demonstrate that Cu/Rh catalyst shows promising catalytic performance for PROX.

■ ASSOCIATED CONTENT

Supporting Information

The Supporting Information is available free of charge at https://pubs.acs.org/doi/10.1021/acs.jpcc.1c04645.

Optimized structures of intermediates and transition states and the calculated barriers and reaction energies. Energy variations of surface Cu atoms exchange with subsurface/bulk Rh atoms. Optimized structures of the Cu_2O overlayer and partially reduced Cu_4O_1 overlayer (PDF)

■ AUTHOR INFORMATION

Corresponding Authors

Wei-Xue Li − *Department of Chemical Physics, School of Chemistry and Materials Science, University of Science and Technology of China, Hefei, Anhui 230026, China;* orcid.org/0000-0002-5043-3088; Email: wxli70@ustc.edu.cn

Xiang-Kui Gu − *School of Power and Mechanical Engineering, Wuhan University, Wuhan 430072, China;* orcid.org/0000-0001-6537-7026; Email: xiangkuigu@whu.edu.cn

Author

Chuwei Zhu − *Department of Chemical Physics, School of Chemistry and Materials Science, University of Science and Technology of China, Hefei, Anhui 230026, China*

Complete contact information is available at: https://pubs.acs.org/10.1021/acs.jpcc.1c04645

Notes

The authors declare no competing financial interest.

■ ACKNOWLEDGMENTS

This work was supported by the National Natural Science Foundation of China (91945302), the National Key R&D Program of China (2018YFA0208603), Chinese Academy of Sciences (QYZDJ-SSW-SLH054), K. C. Wong Education (GJTD-2020-15), and the Dalian National Laboratory for Clean Energy Cooperation Fund (DNL201920). The authors also gratefully thank Supercomputing Center of University of Science and Technology of China and Wuhan University.

■ REFERENCES

(1) Mehta, V.; Cooper, J. S. Review and analysis of PEM fuel cell design and manufacturing. *J. Power Sources* **2003**, *114*, 32−53.

(2) Gu, X.-K.; Li, W.-X. First-Principles Study on the Origin of the Different Selectivities for Methanol Steam Reforming on Cu(111) and Pd(111). *J. Phys. Chem. C* **2010**, *114*, 21539−21547.

(3) Gu, X.-K.; Qiao, B.; Huang, C.-Q.; Ding, W.-C.; Sun, K.; Zhan, E.; Zhang, T.; Liu, J.; Li, W.-X. Supported Single Pt_1/Au_1 Atoms for Methanol Steam Reforming. *ACS Catal.* **2014**, *4*, 3886−3890.

(4) Park, E. D.; Lee, D.; Lee, H. C. Recent progress in selective CO removal in a H_2-rich stream. *Catal. Today* **2009**, *139*, 280−290.

(5) Trimm, D. L. Minimisation of carbon monoxide in a hydrogen stream for fuel cell application. *Appl. Catal., A* **2005**, *296*, 1−11.

(6) Liu, K.; Wang, A.; Zhang, T. Recent Advances in Preferential Oxidation of CO Reaction over Platinum Group Metal Catalysts. *ACS Catal.* **2012**, *2*, 1165−1178.

(7) Bion, N.; Epron, F.; Moreno, M.; Mariño, F.; Duprez, D. Preferential Oxidation of Carbon Monoxide in the Presence of Hydrogen (PROX) over Noble Metals and Transition Metal Oxides: Advantages and Drawbacks. *Top. Catal.* **2008**, *51*, 76.

(8) Manasilp, A.; Gulari, E. Selective CO oxidation over Pt/alumina catalysts for fuel cell applications. *Appl. Catal., B* **2002**, *37*, 17−25.

(9) Zhou, S.; Yuan, Z.; Wang, S. Selective CO oxidation with real methanol reformate over monolithic Pt group catalysts: PEMFC applications. *Int. J. Hydrogen Energy* **2006**, *31*, 924−933.

(10) Snytnikov, P. V.; Sobyanin, V. A.; Belyaev, V. D.; Tsyrulnikov, P. G.; Shitova, N. B.; Shlyapin, D. A. Selective oxidation of carbon monoxide in excess hydrogen over Pt-, Ru- and Pd-supported catalysts. *Appl. Catal., A* **2003**, *239*, 149−156.

(11) Ren, S.; Hong, X. CO selective oxidation in hydrogen-rich gas over platinum catalysts. *Fuel Process. Technol.* **2007**, *88*, 383−386.

(12) Lin, J.; Wang, X.; Zhang, T. Recent progress in CO oxidation over Pt-group-metal catalysts at low temperatures. *Chin. J. Catal.* **2016**, *37*, 1805−1813.

(13) Chen, G.; Yuan, Q.; Li, H.; Li, S. CO selective oxidation in a microchannel reactor for PEM fuel cell. *Chem. Eng. J.* **2004**, *101*, 101−106.

(14) Galletti, C.; Fiorot, S.; Specchia, S.; Saracco, G.; Specchia, V. Activity of rhodium-based catalysts for CO preferential oxidation in H_2-rich gases. *Top. Catal.* **2007**, *45*, 15−19.

(15) Han, Y. F.; Kahlich, M. J.; Kinne, M.; Behm, R. J. CO removal from realistic methanol reformate via preferential oxidation—performance of a Rh/MgO catalyst and comparison to $Ru/\gamma\text{-}Al_2O_3$, and $Pt/\gamma\text{-}Al_2O_3$. *Appl. Catal., B* **2004**, *50*, 209−218.

(16) Echigo, M.; Tabata, T. A study of CO removal on an activated Ru catalyst for polymer electrolyte fuel cell applications. *Appl. Catal., A* **2003**, *251*, 157−166.

(17) Echigo, M.; Tabata, T. Reaction and Surface Characterization Studies of Ru/Al_2O_3 Catalysts for CO Preferential Oxidation in Reformed Gas. *Catal. Lett.* **2004**, *98*, 37−42.

(18) Echigo, M.; Tabata, T. Development of novel Ru catalyst of preferential CO oxidation for residential polymer electrolyte fuel cell systems. *Catal. Today* **2004**, *90*, 269−275.

(19) Lin, J.; Li, L.; Huang, Y.; Zhang, W.; Wang, X.; Wang, A.; Zhang, T. In Situ Calorimetric Study: Structural Effects on Adsorption and Catalytic Performances for CO Oxidation over Ir-in-CeO_2 and Ir-on-CeO_2 Catalysts. *J. Phys. Chem. C* **2011**, *115*, 16509−16517.

(20) Fu, Q.; Li, W.-X.; Yao, Y.; Liu, H.; Su, H.-Y.; Ma, D.; Gu, X.-K.; Chen, L.; Wang, Z.; Zhang, H.; Wang, B.; Bao, X. Interface-Confined Ferrous Centers for Catalytic Oxidation. *Science* **2010**, *328*, 1141−1144.

(21) Mariño, F.; Descorme, C.; Duprez, D. Noble metal catalysts for the preferential oxidation of carbon monoxide in the presence of hydrogen (PROX). *Appl. Catal., B* **2004**, *54*, 59−66.

(22) Pozdnyakova, O.; Teschner, D.; Wootsch, A.; Krohnert, J.; Steinhauer, B.; Sauer, H.; Toth, L.; Jentoft, F. C.; Knop-Gericke, A.; Paal, Z. Preferential CO oxidation in hydrogen (PROX) on ceria-supported catalysts, part I: Oxidation state and surface species on Pt/CeO_2 under reaction conditions. *J. Catal.* **2006**, *237*, 1−16.
(23) Pozdnyakova-Tellinger, O.; Teschner, D.; Kröhnert, J.; Jentoft, F. C.; Knop-Gericke, A.; Schlögl, R.; Wootsch, A. Surface Water-Assisted Preferential CO Oxidation on Pt/CeO_2 Catalyst. *J. Phys. Chem. C* **2007**, *111*, 5426−5431.
(24) Teschner, D.; Wootsch, A.; Pozdnyakova-Tellinger, O.; Kröhnert, J.; Vass, E. M.; Hävecker, M.; Zafeiratos, S.; Schnörch, P.; Jentoft, P. C.; Knop-Gericke, A. Partial pressure dependent in situ spectroscopic study on the preferential CO oxidation in hydrogen (PROX) over Pt/ceria catalysts. *J. Catal.* **2007**, *249*, 318−327.
(25) Roh, H.-S.; Potdar, H. S.; Jun, K.-W.; Han, S. Y.; Kim, J.-W. Low Temperature Selective CO Oxidation in Excess of H_2 over Pt/Ce—ZrO_2 Catalysts. *Catal. Lett.* **2004**, *93*, 203−207.
(26) Wootsch, A.; Descorme, C.; Duprez, D. Preferential oxidation of carbon monoxide in the presence of hydrogen (PROX) over ceria−zirconia and alumina-supported Pt catalysts. *J. Catal.* **2004**, *225*, 259−266.
(27) Zhang, W.; Huang, Y.; Wang, J.; Liu, K.; Wang, X.; Wang, A.; Zhang, T. $IrFeO_x/SiO_2$—A highly active catalyst for preferential CO oxidation in H_2. *Int. J. Hydrogen Energy* **2010**, *35*, 3065−3071.
(28) Qiao, B.; Wang, A.; Yang, X.; Allard, L. F.; Jiang, Z.; Cui, Y.; Liu, J.; Li, J.; Zhang, T. Single-atom catalysis of CO oxidation using Pt_1/FeO_x. *Nat. Chem.* **2011**, *3*, 634−641.
(29) Qiao, B.; Wang, A.; Li, L.; Lin, Q.; Wei, H.; Liu, J.; Zhang, T. Ferric oxide-supported Pt subnano clusters for preferential oxidation of CO in H_2-rich gas at room temperature. *ACS Catal.* **2014**, *4*, 2113−2117.
(30) Minemura, Y.; Ito, S.; Miyao, T.; Naito, S.; Tomishige, K.; Kunimori, K. Preferential CO oxidation promoted by the presence of H_2 over K-Pt/Al_2O_3. *Chem. Commun.* **2005**, 1429−1431.
(31) Minemura, Y.; Kuriyama, M.; Ito, S.-i.; Tomishige, K.; Kunimori, K. Additive effect of alkali metal ions on preferential CO oxidation over Pt/Al_2O_3. *Catal. Commun.* **2006**, *7*, 623−626.
(32) Kuriyama, M.; Tanaka, H.; Ito, S.-i.; Kubota, T.; Miyao, T.; Naito, S.; Tomishige, K.; Kunimori, K. Promoting mechanism of potassium in preferential CO oxidation on Pt/Al_2O_3. *J. Catal.* **2007**, *252*, 39−48.
(33) Tanaka, H.; Kuriyama, M.; Ishida, Y.; Ito, S.-i.; Tomishige, K.; Kunimori, K. Preferential CO oxidation in hydrogen-rich stream over Pt catalysts modified with alkali metals: Part I. Catalytic performance. *Appl. Catal., A* **2008**, *343*, 117−124.
(34) Zhang, W.; Wang, A.; Li, L.; Wang, X.; Zhang, T. Promoting Role of Fe in the Preferential Oxidation of CO Over Ir/Al_2O_3. *Catal. Lett.* **2008**, *121*, 319−323.
(35) Dupont, C.; Jugnet, Y.; Loffreda, D. Theoretical Evidence of PtSn Alloy Efficiency for CO Oxidation. *J. Am. Chem. Soc.* **2006**, *128*, 9129−9136.
(36) Dupont, C.; Delbecq, F.; Loffreda, D.; Jugnet, Y. Preferential CO oxidation in a large excess of hydrogen on Pt3Sn surfaces. *J. Catal.* **2011**, *278*, 239−245.
(37) Komatsu, T.; Tamura, A. Pt3Co and PtCu intermetallic compounds: Promising catalysts for preferential oxidation of CO in excess hydrogen. *J. Catal.* **2008**, *258*, 306−314.
(38) Mu, R.; Fu, Q.; Xu, H.; Zhang, H.; Huang, Y.; Jiang, Z.; Zhang, S.; Tan, D.; Bao, X. Synergetic Effect of Surface and Subsurface Ni Species at Pt-Ni Bimetallic Catalysts for CO Oxidation. *J. Am. Chem. Soc.* **2011**, *133*, 1978−1986.
(39) Ko, E.-Y.; Park, E. D.; Seo, K. W.; Lee, H. C.; Lee, D.; Kim, S. Pt−Ni/γ-Al2O3 catalyst for the preferential CO oxidation in the hydrogen stream. *Catal. Lett.* **2006**, *110*, 275−279.
(40) Khobragade, R.; Yearwar, D.; Labhsetwar, N.; Saravanan, G. Alumina supported nano-platinum on copper nanoparticles prepared via galvanic displacement reaction for preferential carbon monoxide oxidation in presence of hydrogen. *Int. J. Hydrogen Energy* **2019**, *44*, 28757−28768.
(41) Wang, S.-S.; Jian, M.-Z.; Su, H.-Y.; Li, W.-X. First-Principles microkinetic study of methanol synthesis on Cu(221) and ZnCu(221) surfaces. *Chin. J. Chem. Phys.* **2018**, *31*, 284−290.
(42) Cao, K.; Liu, X.; Zhu, Q.; Shan, B.; Chen, R. Atomically Controllable Pd@Pt Core-Shell Nanoparticles towards Preferential Oxidation of CO in Hydrogen Reactions Modulated by Platinum Shell Thickness. *ChemCatChem* **2016**, *8*, 326−330.
(43) Cao, L.; Liu, W.; Luo, Q.; Yin, R.; Wang, B.; Weissenrieder, J.; Soldemo, M.; Yan, H.; Lin, Y.; Sun, Z.; Ma, C.; Zhang, W.; Chen, S.; Wang, H.; Guan, Q.; Yao, T.; Wei, S.; Yang, J.; Lu, J. Atomically dispersed iron hydroxide anchored on Pt for preferential oxidation of CO in H_2. *Nature* **2019**, *565*, 631−635.
(44) Fukuoka, A.; Kimura, J.-i.; Oshio, T.; Sakamoto, Y.; Ichikawa, M. Preferential Oxidation of Carbon Monoxide Catalyzed by Platinum Nanoparticles in Mesoporous Silica. *J. Am. Chem. Soc.* **2007**, *129*, 10120−10125.
(45) Nilekar, A. U.; Alayoglu, S.; Eichhorn, B.; Mavrikakis, M. Preferential CO Oxidation in Hydrogen: Reactivity of Core-Shell Nanoparticles. *J. Am. Chem. Soc.* **2010**, *132*, 7418−7428.
(46) Zhao, S.; Yue, H.; Zhao, Y.; Wang, B.; Geng, Y.; Lv, J.; Wang, S.; Gong, J.; Ma, X. Chemoselective synthesis of ethanol via hydrogenation of dimethyl oxalate on Cu/SiO2: Enhanced stability with boron dopant. *J. Catal.* **2013**, *297*, 142−150.
(47) Natesakhawat, S.; Ohodnicki, P. R., Jr.; Howard, B. H.; Lekse, J. W.; Baltrus, J. P.; Matranga, C. Adsorption and Deactivation Characteristics of Cu/ZnO-Based Catalysts for Methanol Synthesis from Carbon Dioxide. *Top. Catal.* **2013**, *56*, 1752−1763.
(48) van den Berg, R.; Zečević, J.; Sehested, J.; Helveg, S.; de Jongh, P. E.; de Jong, K. P. Impact of the synthesis route of supported copper catalysts on the performance in the methanol synthesis reaction. *Catal. Today* **2016**, *272*, 87−93.
(49) Goncalves, R. V.; Wojcieszak, R.; Wender, H.; Sato, B. D. C.; Vono, L. L.; Eberhardt, D.; Teixeira, S. R.; Rossi, L. M. Easy Access to Metallic Copper Nanoparticles with High Activity and Stability for CO Oxidation. *ACS Appl. Mater. Interfaces* **2015**, *7*, 7987−94.
(50) Pillai, U. R.; Deevi, S. Room temperature oxidation of carbon monoxide over copper oxide catalyst. *Appl. Catal., B* **2006**, *64*, 146−151.
(51) Yang, F.; Graciani, J.; Evans, J.; Liu, P.; Hrbek, J.; Sanz, J. F.; Rodriguez, J. A. CO oxidation on inverse CeO_x/Cu(111) catalysts: high catalytic activity and ceria-promoted dissociation of O_2. *J. Am. Chem. Soc.* **2011**, *133*, 3444−51.
(52) Zeng, S.; Liu, K.; Zhang, L.; Qin, B.; Chen, T.; Yin, Y.; Su, H. Deactivation analyses of CeO_2/CuO catalysts in the preferential oxidation of carbon monoxide. *J. Power Sources* **2014**, *261*, 46−54.
(53) Baber, A. E.; Yang, X.; Kim, H. Y.; Mudiyanselage, K.; Soldemo, M.; Weissenrieder, J.; Senanayake, S. D.; Al-Mahboob, A.; Sadowski, J. T.; Evans, J.; Rodriguez, J. A.; Liu, P.; Hoffmann, F. M.; Chen, J. G.; Stacchiola, D. J. Stabilization of catalytically active Cu^+ surface sites on titanium-copper mixed-oxide films. *Angew. Chem., Int. Ed.* **2014**, *53*, 5336−40.
(54) Jampa, S.; Wangkawee, K.; Tantisriyanurak, S.; Changpradit, J.; Jamieson, A. M.; Chaisuwan, T.; Luengnaruemitchai, A.; Wongkasemjit, S. High performance and stability of copper loading on mesoporous ceria catalyst for preferential oxidation of CO in presence of excess of hydrogen. *Int. J. Hydrogen Energy* **2017**, *42*, 5537−5548.
(55) Won Park, J.; Hyeok Jeong, J.; Yoon, W. L.; Kim, C. S.; Lee, D. K.; Park, Y.-K.; Rhee, Y. W. Selective oxidation of CO in hydrogen-rich stream over Cu−Ce catalyst promoted with transition metals. *Int. J. Hydrogen Energy* **2005**, *30*, 209−220.
(56) Kydd, R.; Ferri, D.; Hug, P.; Scott, J.; Teoh, W. Y.; Amal, R. Temperature-induced evolution of reaction sites and mechanisms during preferential oxidation of CO. *J. Catal.* **2011**, *277*, 64−71.
(57) Caputo, T.; Lisi, L.; Pirone, R.; Russo, G. On the role of redox properties of CuO/CeO_2 catalysts in the preferential oxidation of CO in H_2 rich gases. *Appl. Catal., A* **2008**, *348*, 42−53.
(58) Eren, B.; Heine, C.; Bluhm, H.; Somorjai, G. A.; Salmeron, M. Catalyst Chemical State during CO Oxidation Reaction on Cu(111)

https://doi.org/10.1021/acs.jpcc.1c04645
J. Phys. Chem. C 2021, 125, 19697−19705

Studied with Ambient-Pressure X-ray Photoelectron Spectroscopy and Near Edge X-ray Adsorption Fine Structure Spectroscopy. *J. Am. Chem. Soc.* **2015**, *137*, 11186−90.
(59) Bu, Y.; Niemantsverdriet, J. W. H.; Fredriksson, H. O. A. Cu Model Catalyst Dynamics and CO Oxidation Kinetics Studied by Simultaneous in Situ UV−Vis and Mass Spectroscopy. *ACS Catal.* **2016**, *6*, 2867−2876.
(60) Bu, Y.; Er, S.; Niemantsverdriet, J. W.; Fredriksson, H. O. A. Preferential oxidation of CO in H_2 on Cu and Cu/CeO_x catalysts studied by in situ UV−Vis and mass spectrometry and DFT. *J. Catal.* **2018**, *357*, 176−187.
(61) Huang, T.-J.; Tsai, D.-H. CO Oxidation Behavior of Copper and Copper Oxides. *Catal. Lett.* **2003**, *87*, 173−178.
(62) Jernigan, G. G.; Somorjai, G. A. Carbon Monoxide Oxidation over Three Different Oxidation States of Copper: Metallic Copper, Copper (I) Oxide, and Copper (II) Oxide - A Surface Science and Kinetic Study. *J. Catal.* **1994**, *147*, 567−577.
(63) Gamarra, D.; Belver, C.; Fernández-García, M.; Martínez-Arias, A. Selective CO Oxidation in Excess H_2 over Copper-Ceria Catalysts: Identification of Active Entities/Species. *J. Am. Chem. Soc.* **2007**, *129*, 12064−12065.
(64) Perdew, J. P.; Burke, K.; Ernzerhof, M. Generalized gradient approximation made simple. *Phys. Rev. Lett.* **1996**, *77*, 3865−3868.
(65) Kresse, G.; Joubert, D. From ultrasoft pseudopotentials to the projector augmented-wave method. *Phys. Rev. B: Condens. Matter Mater. Phys.* **1999**, *59*, 1758−1775.
(66) Blochl, P. E. Projector Augmented-Wave Method. *Phys. Rev. B: Condens. Matter Mater. Phys.* **1994**, *50*, 17953−17979.
(67) Henkelman, G.; Uberuaga, B. P.; Jonsson, H. A climbing image nudged elastic band method for finding saddle points and minimum energy paths. *J. Chem. Phys.* **2000**, *113*, 9901−9904.
(68) Henkelman, G.; Jónsson, H. Improved tangent estimate in the nudged elastic band method for finding minimum energy paths and saddle points. *J. Chem. Phys.* **2000**, *113*, 9978−9985.
(69) Henkelman, G.; Jónsson, H. A dimer method for finding saddle points on high dimensional potential surfaces using only first derivatives. *J. Chem. Phys.* **1999**, *111*, 7010−7022.
(70) van den Berg, R.; Parmentier, T. E.; Elkjær, C. F.; Gommes, C. J.; Sehested, J.; Helveg, S.; de Jongh, P. E.; de Jong, K. P. Support Functionalization To Retard Ostwald Ripening in Copper Methanol Synthesis Catalysts. *ACS Catal.* **2015**, *5*, 4439−4448.
(71) Twigg, M. V.; Spencer, M. S. Deactivation of supported copper metal catalysts for hydrogenation reactions. *Appl. Catal., A* **2001**, *212*, 161−174.
(72) Shan, B.; Kapur, N.; Hyun, J.; Wang, L.; Nicholas, J. B.; Cho, K. CO-Coverage-Dependent Oxygen Dissociation on Pt(111) Surface. *J. Phys. Chem. C* **2009**, *113*, 710−715.
(73) Kuittinen, R.-L.; Laasonen, K. Coadsorption of CO and O_2 on Pd(111). *Chem. Phys.* **2005**, *314*, 19−24.
(74) Molina, L. M.; Hammer, B. Theoretical study of CO oxidation on Au nanoparticles supported by MgO(100). *Phys. Rev. B: Condens. Matter Mater. Phys.* **2004**, *69*, 155424.
(75) Yuan, D. W.; Liu, Z. R.; Chen, J. H. Catalytic activity of Pd ensembles over Au(111) surface for CO oxidation: A first-principles study. *J. Chem. Phys.* **2011**, *134*, 054704.
(76) Liu, Y.; Li, H.; Cen, W.; Li, J.; Wang, Z.; Henkelman, G. A computational study of supported Cu-based bimetallic nanoclusters for CO oxidation. *Phys. Chem. Chem. Phys.* **2018**, *20*, 7508−7513.
(77) Ruban, A. V.; Skriver, H. L.; Norskov, J. K. Surface segregation energies in transition-metal alloys. *Phys. Rev. B: Condens. Matter Mater. Phys.* **1999**, *59*, 15990−16000.
(78) Wang, L.-L.; Johnson, D. D. Predicted Trends of Core-Shell Preferences for 132 Late Transition-Metal Binary-Alloy Nanoparticles. *J. Am. Chem. Soc.* **2009**, *131*, 14023−14029.

https://doi.org/10.1021/acs.jpcc.1c04645
J. Phys. Chem. C 2021, 125, 19697−19705